Front. Earth Sci. 2023, 17(3): 832−843
https://doi.org/10.1007/s11707-022-1029-7

RESEARCH ARTICLE

Reasonable start time of carbon dioxide injection in enhanced coalbed methane recovery involving thermal-hydraulic-mechanical couplings

Chaojun FAN[1], Lei YANG (✉)[1], Bin XIAO[1], Lijun ZHOU[2], Haiou WEN[1], Hao SUN[1]

1 College of Mining, Liaoning Technical University, Fuxin 123000, China
2 College of Safety Science and Engineering, Liaoning Technical University, Huludao 125105, China

Abstract Injection of gas (CO_2) into coal seams is an effective method to benefit from both CO_2 geological storage and coalbed methane recovery. Based on the dual pore structure of coal mass, and the Weibull distribution of fracture permeability, a thermal-hydraulic-mechanical (THM) coupling mathematical model is proposed involving the non-isothermal adsorption of binary gases, dynamic gas diffusion between matrix and fractures, multiphase seepage, coal deformation, heat conduction and heat convection. This mathematical model is applied to study the process of CO_2-enhanced coalbed methane recovery (CO_2-ECBM). Results show that the CH_4 content of CO_2-ECBM in coal seam decreases significantly when compared with that of regular drainage, and decreases rapidly in the early stage but slowly in the later stage. Coal seam permeability evolution is triggered by changes in gas adsorption/desorption, temperature and effective stress. For regular drainage, the early permeability shows a decreasing trend dominated by the increase of effective stress, while the later permeability shows an increasing trend dominated by the CH_4 desorption caused shrinkage of coal matrix. For CO_2-ECBM, the permeability in coal seam generally shows a downward trend due to both matrix swelling induced by gas adsorption and thermal expansion, particularly near injection well. There appears an increased and delayed peak production rate of CH_4. The CH_4 production rate of CO_2-ECBM is always higher than that of regular drainage. The CH_4 cumulative production and CO_2 cumulative storage linearly increase with time, and the CH_4 cumulative production of CO_2-ECBM increased by 39.2% in the duration of 5000 d compared with regular drainage. Reasonable CO_2 injection starting time can overcome the issue of early CO_2 breakthrough and ineffective increase of CH_4 production. In the studied case, the optimal injection starting time is 2500 d. Compared with the simultaneous CH_4 extraction and CO_2 injection, the CH_4 cumulative production of optimal time has increased by 30.1%. The research provides a reference for determining the reasonable CO_2 injection time under similar conditions.

Keywords CO_2 sequestration, coalbed methane, reasonable injection start time, thermo-hydro-mechanical coupling model, numerical simulation

1 Introduction

Coalbed methane (CH_4) is a greenhouse and disastrous gas, which holds 25 times greenhouse effect of the carbon dioxide (CO_2) and may cause gas explosion, coal and gas outburst during coal mining (Liu et al., 2021a). Meanwhile, coalbed methane is also an unconventional gas resource. The low permeability and the complex occurrences of China's coal seams greatly limit the efficiency of coalbed methane recovery (Zhu et al., 2022). Under the goal of carbon neutrality and carbon peaking, injecting CO_2 into the coal seam to enhance coalbed methane recovery (CO_2-ECBM) cannot only improve the recovery rate of coalbed methane, but also help reduce carbon emissions (Liu et al., 2019).

Since proposed the concept of CO_2 injection to improve coalbed methane extraction efficiency, scholars have carried out a large number of experiments and numerical simulations on CO_2-ECBM. The United States carried out the first CO_2-ECBM field test in the San Juan Basin. Since then, Canada and China have carried out tests in the Alberta and Qinshui Coalfields, along with the similar tests conducted in Japan, Poland and Australia (Fang et al., 2019a). Zhang et al. (2021) conducted experiments

Received May 25, 2022; accepted August 30, 2022

E-mail: leiyang106@163.com

on core injection of N_2 and CO_2 to displace coalbed methane, and found that the recovery rate of coalbed methane with CO_2 injection is higher (Zhou et al., 2013). Zheng et al. (2020) obtained that the injected CO_2 will compete with CH_4 on the adsorption site to replace the CH_4 in the coal seam due to the stronger sorption affinity of CO_2 on coal, by means of nuclear magnetic resonance (NMR) test (Liu et al., 2017). This process is affected by factors such as injection pressure, confining pressure, temperature, permeability and adsorption capacity (Sun et al., 2018; Liu et al., 2022). And coal permeability and sorption affinity are the determinants of CO_2 injection capacity and sequestration capacity, respectively (Niu et al., 2020). The CO_2 sequestration and CH_4 production of high-rank coal are higher than those of low-rank coal (Zhang and Ranjith, 2019; Zheng et al., 2022). Numerical simulations of CO_2-ECBM have been extensively studied in order to provide reference to field tests. Fan et al. (2019a) established a thermo-hydro-mechanical (THM) model including the governing equations of coal deformation, fluid seepage, diffusion and heat transport, and solved by the finite element method to simulate the CO_2-ECBM recovery. Based on the mathematical model, the effects of adsorption time (Vishal et al., 2015), injection pressure and temperature (Mu et al., 2019; Hou et al., 2020) and diffusion coefficient (Sun et al., 2018) on gas production during CO_2-ECBM process have been explored. Similarly, studies have proven that coal permeability is the dominant factor affecting CO_2 injection and CH_4 production (Liu et al., 2011), and changes in matrix expansion, contraction and effective stress are the key factors on permeability (Fang et al., 2019b). The have improved the theoretical level of CO_2-ECBM and promoted its technological progress. However, the existence of water in the coal seam will reduce the relative permeability of gas and hinders the extraction of coalbed methane (Wang et al., 2022). In addition, premature CO_2 injection will cause premature breakthrough and reduce the calorific value in the extracted gas, and the appropriate CO_2 injection time needs to be further studied.

In this paper, coal mass is considered as a dual-porosity (pores and fractures) material, and Weibull distribution based permeability. A thermo-hydro-mechanical coupled mathematical model is proposed by considering non-isothermal adsorption of binary gases (CH_4, CO_2), dynamic diffusion between matrix and fracture, multi-phase seepage, coal deformation, heat conduction and heat convection. On the background of Qinshui Basin in China, numerical solution of the mathematical model by COMSOL Multiphysics software is obtained. The CO_2-ECBM recovery process is studied and the reasonable time of CO_2 injection was determined. It provides a reference for improving the efficiency of CO_2-ECBM in coal seams.

2 Mathematical model for CO_2-ECBM in coal seam

2.1 Basic assumptions

Based on the basic characteristics of gas and water existing in coal seam, the following assumptions are made (Cheng et al., 2021; Liu et al., 2021b; Xiao et al., 2021; Zhao et al., 2022). 1) The coal mass is an elastic medium with dual porosity (pore-fracture) and single permeability structure, and the initial permeability satisfies the Weibull distribution. 2) Gas (CH_4 and CO_2) transport in the matrix satisfies Fick's diffusion law, while the gas transport in the fracture satisfies Darcy's seepage law. 3) Water only transports in fracture. 4) Both CH_4 and CO_2 are regarded as ideal state gases, satisfying the ideal gas state equation. 5) The gravity of gases is ignored. 6) The tensile stress is positive and the compressive stress is negative.

2.2 Governing equations for fluid transport field

2.2.1 Gas transport with in coal matrix

According to the ideal gas state equation, the gas density of each component under standard conditions is (Fang et al., 2019a)

$$\rho_{gsi} = \frac{M_{gi}}{RT_s} p_s, \tag{1}$$

where $i = 1$ represents CH_4, $i = 2$ represents CO_2; M_{gi} is the molar mass of gas component i, g/mol; R is the gas molar constant, J/(mol·K); T is the coal seam temperature, K; T_s is the standard temperature; p_s is the standard atmospheric pressure, kPa.

The modified Langmuir adsorption equation is adopted to express the adsorbed gas content per unit coal matrix at variable temperature is (Huo et al., 2019)

$$V_{sgi} = \frac{V_{Li} b_i P_{mgi}}{1 + \sum_{i=1}^{2} b_i P_{mgi}} \exp\left[-\frac{c_1}{1 + c_2 p_m}(T - T_{ref})\right], \tag{2}$$

where V_{Li} is the Langmuir volume constant of gas component i, m^3/kg; P_{Li} is the Langmuir pressure constant of component i, Pa; $b_i = 1/P_{Li}$; p_{mgi} is the pressure of component i in the matrix, Pa; c_1 is the temperature coefficient, 1/K; c_2 is the pressure coefficient, 1/Pa; $p_m = p_{mg1} + p_{mg2}$, is the gas pressure in the matrix, Pa; T_{ref} is the reference temperature in the adsorption/desorption experiment, K.

The gas content per unit volume of coal matrix is the sum of free gas content and adsorbed gas content (Fan et al., 2018):

$$m_{mgi} = \phi_m \frac{M_{gi}}{RT} p_{mgi} + V_{sgi} \rho_c \frac{M_{gi}}{RT_s} p_s, \tag{3}$$

where ϕ_m is the initial matrix porosity; V_{sgi} is the

adsorbed gas content of component i, m^3/kg; ρ_c is the true density of coal, kg/m^3.

At beginning, gas (CH_4) in coal seam is dynamically balanced between adsorption and desorption, and the gas pressure in the matrix is equal to the gas pressure in fracture. The original equilibrium will be broken under the action of extraction and gas injection, and the gas in the coal matrix transport by means of diffusion driven by the concentration gradient. According to Fick's diffusion law, the gas mass conservation equation in the matrix can be obtained as (Fan et al., 2017)

$$\frac{\partial m_{\mathrm{mg}i}}{\partial t} = -\frac{M_{\mathrm{g}i}}{\tau_i RT}\left(p_{\mathrm{mg}i} - p_{\mathrm{fg}i}\right), \tag{4}$$

where τ_i is the desorption time of gas component i; $p_{\mathrm{fg}i}$ is the pressure of gas component i in the fracture, Pa.

Substituting Eqs. (1)−(3) into Eq. (4), the gas transport equation in the matrix can be obtained as

$$\frac{\partial}{\partial t}\left(\phi_{\mathrm{m}}\frac{M_{\mathrm{g}i}}{RT}p_{\mathrm{mg}i} + \frac{V_{\mathrm{L}i}b_i P_{\mathrm{mg}i}}{1+\sum_{i=1}^{2} b_i P_{\mathrm{mg}i}}\exp\left[-\frac{c_1}{1+c_2 p_{\mathrm{m}}}(T-T_{\mathrm{ref}})\right] \cdot \frac{M_{\mathrm{g}i}}{RT_{\mathrm{s}}}\rho_{\mathrm{c}} p_{\mathrm{s}}\right) = -\frac{1}{\tau_i}\frac{M_{\mathrm{g}i}}{RT}\left(p_{\mathrm{mg}i} - p_{\mathrm{fg}i}\right). \tag{5}$$

2.2.2 Gas and water transport in fracture

In the process of CO_2 displacing CH_4 in coal seam, the fluid migration is in the state of gas-water two-phase flow. The adsorbed CH_4 on the pore surface of coal matrix desorbs, providing a mass source for the CH_4 migration in the fractures. The CO_2 transport in the fractures acts as a mass sink for the adsorption of CO_2 in the matrix. Therefore, the mass conservation equation of the gas-water two-phase flow in coal seam is defined as follows (Fang et al., 2019c):

$$\begin{cases} \dfrac{\partial\left(s_{\mathrm{g}}\phi_{\mathrm{f}}\rho_{\mathrm{fg}i}\right)}{\partial t} + \nabla\cdot\left(\rho_{\mathrm{fg}i}q_{\mathrm{g}i}\right) = \left(1-\phi_f\right)\dfrac{M_{\mathrm{g}i}}{\tau_i RT}\left(p_{\mathrm{mg}i} - p_{\mathrm{fg}i}\right), \\ \dfrac{\partial\left(s_{\mathrm{w}}\phi_{\mathrm{f}}\rho_{\mathrm{w}}\right)}{\partial t} + \nabla\cdot\left(\rho_{\mathrm{w}}q_{\mathrm{w}}\right) = 0 \end{cases} \tag{6}$$

where s_g is the gas saturation in fracture; s_w is the water saturation in fracture, $s_g + s_w = 1$; ϕ_f is the fracture porosity; q_{gi} is the velocity of gas component i, m/s; q_w is the water velocity, m/s; ρ_w is the density of water under standard conditions, kg/m^3.

Incorporating with the gas slippage effect and gas-water two-phase, the fluid transport speed can be obtained according to the generalized Darcy's law (Fan et al., 2021a):

$$\begin{cases} q_{\mathrm{g}i} = -\dfrac{kk_{\mathrm{rg}}}{\mu_{\mathrm{g}i}}\left(1+\dfrac{b_{\mathrm{k}}}{p_{\mathrm{fg}i}}\right)\nabla p_{\mathrm{fg}i} \\ q_{\mathrm{w}} = -\dfrac{kk_{\mathrm{rw}}}{\mu_{\mathrm{w}}}\nabla p_{\mathrm{fw}} \end{cases}, \tag{7}$$

where k is the absolute permeability in coal, m^2; k_{rg} is the relative permeability of gas; b_k is the Klinkenberg factor, Pa; k_{rw} is the relative permeability of water; μ_{gi} is the dynamic viscosity of gas component i, Pa·s; μ_w is the dynamic viscosity of water, Pa·s, p_{fw} is the pressure of water in the fracture, $p_{fw} = p_{fg} - p_{cgw}$, Pa; p_{cgw} is the capillary pressure, Pa.

The relative permeability model of gas-water two-phase flow is (Luo et al., 2022)

$$\begin{cases} k_{\mathrm{rg}} = k_{\mathrm{rg0}}\left[1-\left(\dfrac{s_{\mathrm{w}}-s_{\mathrm{wr}}}{1-s_{\mathrm{wr}}-s_{\mathrm{gr}}}\right)\right]^2\left[1-\left(\dfrac{s_{\mathrm{w}}-s_{\mathrm{wr}}}{1-s_{\mathrm{wr}}}\right)^2\right] \\ k_{\mathrm{rw}} = k_{\mathrm{rw0}}\left(\dfrac{s_{\mathrm{w}}-s_{\mathrm{wr}}}{1-s_{\mathrm{wr}}}\right)^4 \end{cases}, \tag{8}$$

where k_{rg0} is the relative permeability at the gas phase endpoint; s_w is the water saturation; s_{wr} is the irreducible water saturation; s_{gr} is the residual gas saturation; k_{rw0} is the relative permeability at the water phase endpoint.

By substituting Eqs. (7) and (8) into Eq. (6), the governing equation of gas and transport in fracture can be obtained:

$$\begin{cases} \dfrac{\partial}{\partial t}\left(s_{\mathrm{g}}\phi_{\mathrm{f}}\dfrac{M_{\mathrm{g}i}}{RT}p_{\mathrm{fg}i}\right) + \nabla\cdot\left(-\dfrac{M_{\mathrm{g}i}}{RT}\dfrac{kk_{\mathrm{rg}}\left(p_{\mathrm{fg}i}+b_{\mathrm{k}}\right)}{\mu_{\mathrm{g}i}}\nabla p_{\mathrm{fg}i}\right) \\ \quad = \left(1-\phi_{\mathrm{f}}\right)\dfrac{M_{\mathrm{g}i}}{\tau_i RT}\left(p_{\mathrm{mg}i} - p_{\mathrm{fg}i}\right) \\ \dfrac{\partial\left(s_{\mathrm{w}}\phi_{\mathrm{f}}\rho_{\mathrm{w}}\right)}{\partial t} + \nabla\cdot\left(-\dfrac{\rho_{\mathrm{w}}kk_{\mathrm{rw}}}{\mu_{\mathrm{w}}}\nabla p_{\mathrm{fw}}\right) = 0 \end{cases}. \tag{9}$$

2.3 Governing equations for stress field

Considering the thermal expansion/shrinkage strain, the strain caused by the change of pore and fracture pressure, the shrinkage/expansion strain caused by the adsorption/desorption of CH_4 and CO_2, the total strain of the coal mass is (Xia et al., 2015)

$$\varepsilon_{ij} = \frac{1}{2G}\sigma_{ij} - \left(\frac{1}{6G} - \frac{1}{9K}\right)\sigma_{kk}\delta_{ij} + \frac{\alpha_T T}{3}\delta_{ij} + \frac{\alpha_{\mathrm{m}}p_{\mathrm{m}} + \alpha_{\mathrm{f}}p_{fg}}{3K}\delta_{ij} + \frac{\varepsilon_{\mathrm{a}}}{3}\delta_{ij}, \tag{10}$$

where δ_{ij} is the Kronecker symbol; $G = D/2(1+\nu)$ is the shear modulus of coal, Pa; $D = 1/[(1/E) + 1/(a\cdot K_n)]$ is the effective elastic modulus, Pa; E elastic modulus of coal, Pa; a is the initial matrix width, m; K_n is the fracture stiffness, Pa; ν is the Poisson's ratio of coal; α_m is the pore Biot coefficient, $\alpha_m = 1-K/K_s$; $K = D/3(1-2\nu)$ is the bulk modulus of the coal, Pa; $Ks = Es/3(1-2\nu)$ is the bulk modulus of the coal skeleton, Pa; E_s is the elastic modulus of the coal skeleton, Pa; α_T is coal skeleton thermal expansion coefficient, 1/K; p_m is matrix gas pressure, Pa,

$p_m = p_{mg1} + p_{mg2}$; p_f is fracture fluid pressure, Pa, $p_f = s_w \cdot p_{fw} + s_g \cdot p_{fg}$; $\alpha_f = 1 - K/(a \cdot K_n)$ is the fracture Biot coefficient; $\varepsilon_a = \varepsilon_1 + \varepsilon_2$, is the expansion/shrinkage strain caused by the adsorption/desorption of gas in the coal matrix.

The strain of matrix expansion/shrinkage induced by gas adsorption/desorption in coal can be expressed as (Ren et al., 2017)

$$\varepsilon_{ai} = \frac{\varepsilon_{Li} b_i p_{mgi}}{\left(1 + \sum_{i=1}^{2} b_i p_{mgi}\right)}, \tag{11}$$

where ε_{Li} is the strain constant of the adsorbed gas component i in coal matrix.

According to elastic mechanics, the geometric relationship and static equilibrium relationship of coal reservoir are respectively (Fan et al., 2022):

$$\begin{cases} \varepsilon_{ij} = \dfrac{1}{2}\left(u_{i,j} + u_{j,i}\right) \\ \sigma_{ij,j} + F_i = 0 \end{cases}, \tag{12}$$

where F_i is the body force, Pa; u_i is the displacement in the i direction, m; $i = x, y, z$.

By combining Eqs. (10)−(12), the governing equation of stress field of coal mass can be obtained (Fan et al., 2021b):

$$Gu_{i,jj} + \frac{G}{1-2\nu} u_{j,ji} - K\alpha_T \Delta T_{,i} - \alpha_m p_{m,i} - \alpha_f p_{f,i} - K\varepsilon_{a,i} + F_i = 0. \tag{13}$$

2.4 Governing equations for heat transport field

In the coal seam, coal skeleton, CH_4, and water coexist in a unit volume system. The temperature change causes the internal energy to change. The system exchanges heat with the outside world through thermal convection and heat conduction. The volumetric strain of the coal mass produces deformation. The CH_4 and CO_2 adsorption/desorption process is accompanied by heat release/absorption. According to the law of heat conservation, the governing equation of the heat transport field can be obtained as (Zhou et al., 2022)

$$\frac{\partial\left(\left(\rho C_p\right)_{eff} T\right)}{\partial t} + \eta_{eff}\nabla T - \nabla\cdot\left(\lambda_{eff}\nabla T\right) + K\alpha_T T\frac{\partial \varepsilon_v}{\partial t} + \sum_{i=1}^{2} q_{sti}\frac{\rho_c \rho_{gsi}}{M_{gi}}\frac{\partial V_{sgi}}{\partial t} = 0. \tag{14}$$

Among,

$$\begin{cases} \left(\rho C_p\right)_{eff} = (1-\phi_f-\phi_m)\rho_c C_s + \sum_{i=1}^{2}\left(s_g\phi_f\rho_{fgi} + \phi_m\rho_{mgi}\right)C_{gi} + s_w\phi_f\rho_w C_w \\ \eta_{eff} = -\sum_{i=1}^{2}\left(\dfrac{\rho_{fgi}C_{gi}kk_{rg}}{\mu_{gi}}\left(1+\dfrac{b_k}{p_{fgi}}\right)\nabla p_{fgi} - \dfrac{\rho_w C_w kk_{rw}}{\mu_w}\nabla p_{fw}\right) \\ \lambda_{eff} = (1-\phi_f-\phi_m)\lambda_s + \phi_m\lambda_{mg} + \phi_f\left(s_g\lambda_{fg} + s_w\lambda_{fw}\right) \end{cases}$$

where $(\rho C_p)_{eff}$ is the effective specific heat capacity of the coal, J/(m^3·K); η_{eff} is the effective convection coefficient of the fluid, J/(m^2·s); λ_{eff} is the effective thermal conductivity of the coal, W/(m·K); q_{sti} is the isosteric heat of gas adsorption of component i, J/mol; C_s, C_g, and C_w are the specific heat capacities of the coal skeleton, coalbed methane and water, respectively, J/(kg·K); λ_s, λ_g, and λ_w are the thermal conductivity of coal skeleton, coalbed methane and water, respectively, W/(m·K).

2.5 Porosity and permeability evolution

Coal seam is a dual-porous and single-permeable medium, as shown in Fig. 1. Matrix pores are the main storage space for CH_4 and CO_2, and the fracture change affects the change of permeability. Therefore, the changes of pores and fractures are the key factors in the process of injection of CO_2 to enhance CH_4 drainage. The coal matrix porosity model can be expressed as (Fan et al., 2019b)

$$\phi_m = \frac{(1+S_0)\phi_{m0} + \alpha_m(S - S_0)}{(1+S)}, \tag{15}$$

where ϕ_{m0} is the initial matrix porosity; $S = \varepsilon_v + p_m/K_s - \alpha_T T - \varepsilon_a$; $S_0 = \varepsilon_{v0} + p_{m0}/K_s - \alpha_T T_0 - \varepsilon_{a0}$; ε_v is the volumetric strain; the subscript '0' represents the initial value of the parameter.

Considering the effective stress on the coal matrix and

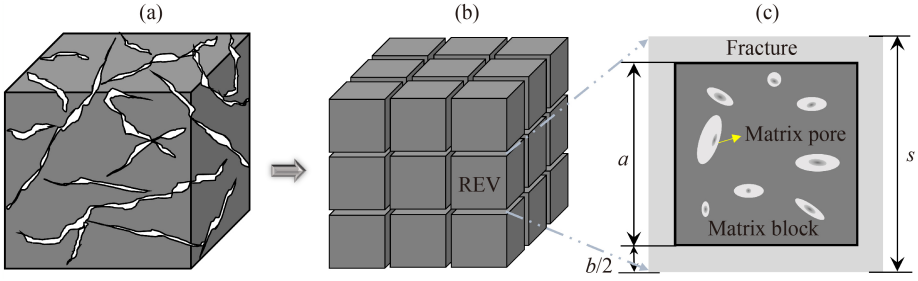

Fig. 1 Physical model of double-porous single-permeability medium. (a) Simplified model of coal; (b) equivalent fracture distribution of coal; (c) representative element volume.

fractures, the volumetric strain of the representative element volume (REV) can be defined as (Wang et al., 2018):

$$\Delta\varepsilon_v = \frac{a^3}{s^3 K_m}\Delta\sigma_{em} + \frac{s^3 - a^3}{s^3 K_f}\Delta\sigma_{ef} - \frac{a^3}{s^3}\Delta\varepsilon_a - \frac{a^3}{s^3}\alpha_T \Delta T. \quad (16)$$

where $s = a + b$, is the width of the REV, m; K_m is the matrix shear modulus, Pa; K_f is the equivalent crack stiffness, Pa; $K_f = bK_n$, b is the initial crack width, m; $\sigma_{em} = -\sigma - (\alpha_m \cdot p_m + \alpha_f \cdot p_f)$, is the effective stress of coal matrix; $-\sigma = (\sigma_1 + \sigma_2 + \sigma_3)/3$, is the average effective stress; $\sigma_{ef} = -\sigma - \alpha_f \cdot p_f$ is the effective stress of coal fracture.

Assuming $r_{as} = a/s$, the effective stress on fracture can be obtained from Eq. (16) as

$$\Delta\sigma_{ef} = \frac{K_m K_f}{K_f r_{as}^3 + K_m - K_m r_{as}^3} \cdot \left(\frac{r_u^3}{K_m}\alpha_m \Delta p_m + r_{as}^3 \Delta\varepsilon_\alpha + r_{as}^3 \alpha_T \Delta T + \Delta\varepsilon_v\right). \quad (17)$$

The deformation of the fracture dominated by the effective stress can be expressed as

$$\Delta b = \frac{b}{3K_f}\Delta\sigma_{ef}. \quad (18)$$

The evolution of fracture porosity can be defined as

$$\phi_f = \phi_{f0}\left(1 + \frac{\Delta b}{b}\right) = \phi_{f0} + \frac{\phi_{f0} K_m}{3\left(K_f r_{as}^3 + K_m - K_m r_{as}^3\right)} \cdot \left(\frac{r_{\alpha s}^3}{K_m}\alpha_m \Delta p_m + r_{as}^3 \Delta\varepsilon_a + r_{as}^3 \alpha_T \Delta T + \Delta\varepsilon_v\right). \quad (19)$$

According to the cubic law, the relationship between fracture porosity and permeability is

$$\frac{k}{k_0} = \left(\frac{\phi_f}{\phi_{f0}}\right)^3, \quad (20)$$

where k_0 is the initial permeability of coal seam, m^2.

Substitute Eq. (19) into Eq. (20) can be obtained the dynamic evolution equation of permeability:

$$k = k_0\left(1 + \frac{K_m}{3\left(K_f r_{as}^3 + K_m - K_m r_{as}^3\right)} \cdot \left(\frac{r_{as}^3}{K_m}\alpha_m \Delta p_m + r_{as}^3 \Delta\varepsilon_a + r_{as}^3 \alpha_T \Delta T + \Delta\varepsilon_v\right)\right)^3. \quad (21)$$

The Eqs. (5), (9), (13), and (14) are assembled together to establish the THM coupling mathematical model of CO_2-ECBM. The solid mechanics module and PDE module of COMSOL Multiphysics are used to jointly solve it numerically.

3 Simulation of CO_2 sequestration and CH_4 enhanced recovery

3.1 Geometry model and definite conditions

Qinshui Basin is one of the coalbed methane basins successfully developed in China. In 2002, the Ministry of Commerce of China and the Canadian International Development Agency (CIDA) jointly conducted a CO_2-ECBM experiment (Wu et al., 2011). In the experiment, the traditional five-point well arrangement with a central injection well (IW) located in the middle and four production wells (PW) at the vertex of an approximate rectangle was adopted. To facilitate numerical simulation, a 150 m × 150 m area between PW and IW was selected for research, as shown in Fig. 2. The No. 3 coal seam in the Qinshui Basin is characterized by a thickness of 5 m, initial CH_4 pressure of 5.24 MPa, water saturation of 0.8, initial temperature of 305.5 K, and initial permeability of 5.14×10^{-16} m^2. The diameter of both gas injection and production wells is 0.1 m. The surrounding of the model

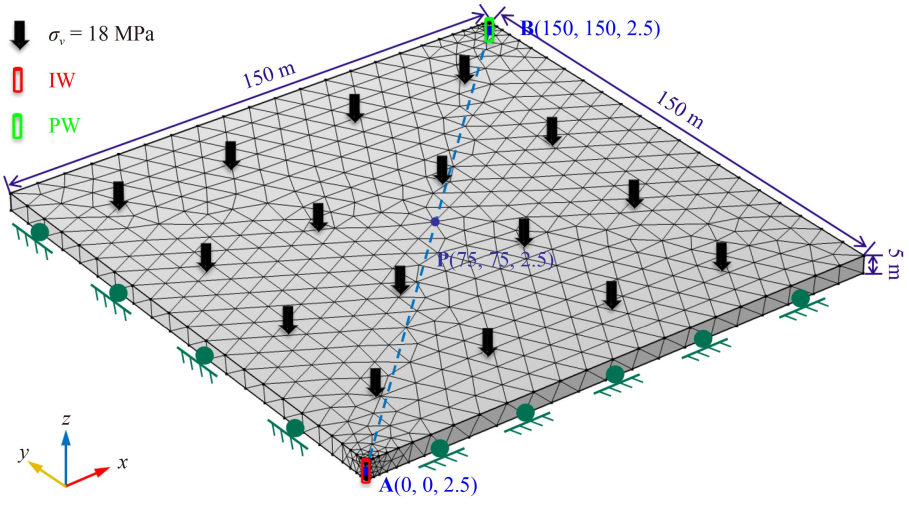

Fig. 2 Geometric model for CO_2-ECBM simulation.

are set as roller boundary condition. The gravity of the overlying rock layer is 18 MPa. There is no flow for both fluid and heat with the outside at the surrounding boundary. The gas pressure on injection well is set as 8 MPa, the pressure in production well is 0.15 MPa. The temperature of the injection flux is 323 K. The reference line A-B and the reference point P are set. The parameters used in the numerical simulation are obtained from the geological data of the No. 3 coal seam in the Qinshui Basin and literature (Fan et al., 2019a), as shown in Table 1.

The Weibull distribution function is introduced to characterize the heterogeneity of the coal permeability (Fan et al., 2017):

$$f(u) = \frac{m}{u_0}(u/u_0)^{m-1}\exp[-(u/u_0)^m], \quad (22)$$

where m is the homogeneity index, and larger homogeneity index corresponds to better uniformity of permeability; u_0 is the average permeability of the REV; u is the permeability of the REV.

The Weibull function based permeability distribution was first generated by MATLAB code, and then imported to COMSOL Multiphysics to calculate the CO_2-ECBM process. Figure 3 is probability distribution of average permeability (k_0 = 5.14 × 10^{-16} m^2) in coal seam with varying homogeneity index. When the value of homogeneity index is small, the permeability distribution is more discrete and distribution range is wider. When the value of homogeneity index is large, the permeability distribution is more concentrated, mainly around the average permeability. The homogeneity index was set as 6 in the following research.

3.2 Results of numerical simulation

3.2.1 Gas content evolution

In Fig. 4, the CH_4 content begins to decrease near the production well, and gradually expands to whole coal seam during regular gas drainage. Under the action of suction pressure caused by drainage, the pressure gradient between reservoir and production well is generated. CH_4 gradually transports to the production well driven by the pressure gradient. Hence, the CH_4 content decreases with time. The closer to the production well, the greater the pressure gradient. Therefore, the CH_4 content decreases more rapidly near the production well. Figure 5 illustrates the evolution of CH_4 content on the reference line AB during regular drainage. The CH_4 content on the reference line AB gradually decreases with time, with faster decreasing rate near the production well.

Table 1 Parameters related to numerical simulation

Parameter	Value	Parameter	Value
Initial CH_4 pressure in fracture (p_{f10}, MPa)	5.24	Specific heat capacity of coal (C_s, J/(kg·K))	1350
Initial CH_4 pressure in matrix (p_{m10}, MPa)	5.24	Specific heat capacity of water (C_w, J/(kg·K))	4187
Initial CO_2 pressure in fracture (p_{f20}, MPa)	0.2	Specific heat capacity of CH_4 (C_{g1}, J/(kg·K))	2220
Initial CO_2 pressure in matrix (p_{m20}, MPa)	0.2	Specific heat capacity of CO_2 (C_{g2}, J/(kg·K))	844
Young's modulus of coal seam (E, MPa)	2815	Density of coal (ρ_c, kg·m^{-3})	1470
Young's modulus of coal skeleton (E_S, MPa)	8469	Klinkenberg factor (b_k, MPa)	0.76
Poisson's ratio of coal (v)	0.32	Relative permeability of water (k_{rw0})	1.0
Fracture stiffness (K_n, GPa/m)	2.8	Relative permeability of gas (k_{rg0})	0.875
Langmuir volume constant of CH_4 (V_{L1}, m^3·kg^{-1})	0.0256	Capillary pressure (p_{cgw}, MPa)	0.035
Langmuir pressure constant of CH_4 (P_{L1}, MPa)	2.07	Adsorption time of CH_4 (τ_1, d)	0.221
Langmuir volume constant of CO_2 (V_{L2}, m^3·kg^{-1})	0.0447	Adsorption time of CO_2 (τ_2, d)	0.334
Langmuir pressure constant of CO_2 (P_{L2}, MPa)	1.38	Initial temperature in coal seam (T_0, K)	305.5
Dynamic viscosity of CH_4 (μ_{g1}, 10^{-5}pa·s)	1.34	Gas molar constant (R, J·mol^{-1}·K^{-1})	8.314
Dynamic viscosity of CO_2 (μ_{g2}, 10^{-5}pa·s)	1.84	Initial porosity of matrix (ϕ_{m0})	0.045
Dynamic viscosity of water (μ_w, 10^{-3}pa·s)	1.01	Initial porosity of fracture (ϕ_{f0})	0.011
Adsorption strain constant of CH_4 (ε_{L1})	0.0128	Initial permeability of fracture (k_0, m^2)	5.14 × 10^{-16}
Adsorption strain constant of CO_2 (ε_{L2})	0.0237	Thermal conductivity of coal (λ_s, W/(m·K))	0.1913
Temperature coefficient (c_1, 1/T)	0.021	Thermal conductivity of CH_4 (λ_{g1}, W/(m·K))	0.0301
Pressure coefficient (c_2, 1/MPa)	0.071	Thermal conductivity of CO_2 (λ_{g2}, W/(m·K))	0.0137
Isosteric heat of CH_4 adsorption (q_{st1}, kJ/mol)	16.4	Initial water saturation (s_{w0})	0.8
Isosteric heat of CO_2 adsorption (q_{st2}, kJ/mol)	19.2	Irreducible water saturation (s_{wr})	0.42

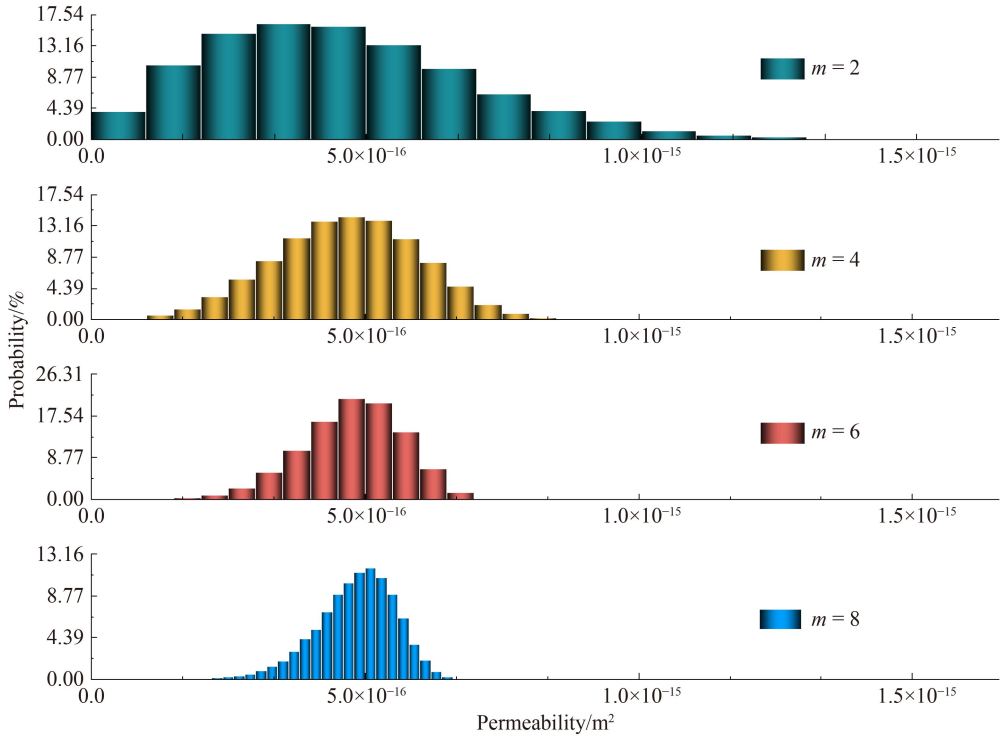

Fig. 3 Probability distribution of coal permeability with various homogeneity index *m*.

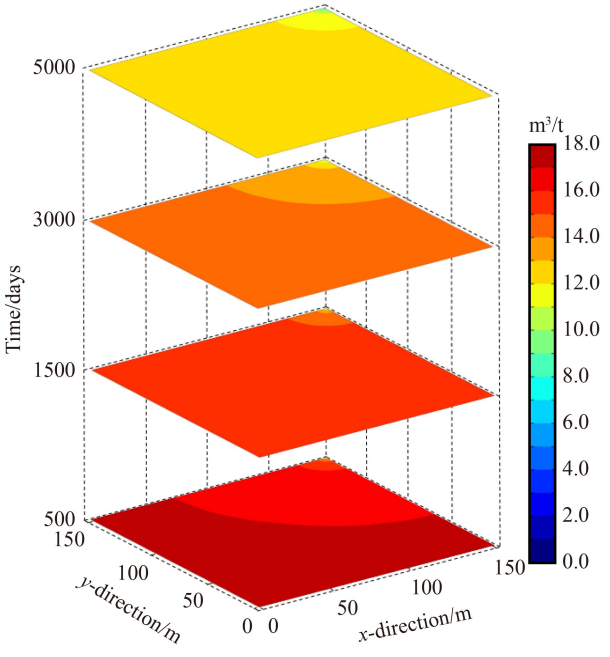

Fig. 4 CH_4 content in coal seam during regular drainage.

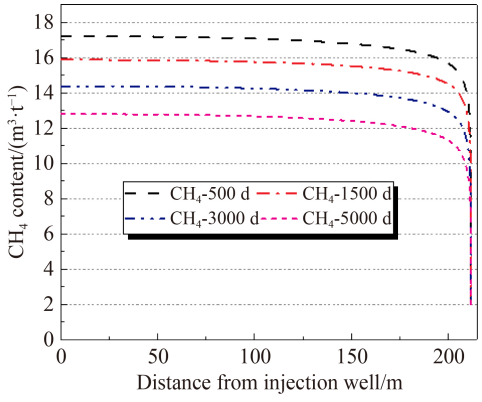

Fig. 5 CH_4 content on the reference line AB during regular drainage.

In Fig. 6, the CH_4 content of CO_2-ECBM decreases more dramatically than that of regular drainage, caused by the persistent injection of CO_2. At point P, CH_4 of regular drainage decrease by 27.8%, from the initial 18.0 m^3/t to 13.0 m^3/t. While, the CH_4 content of CO_2-ECBM decreases by 50.0%, from 18.0 m^3/t to 9.0 m^3/t. The decrease of CH_4 content slower at the later stage compared with the early stage. CH_4 content decreases more dramatically near the injection well than the production well. When CO_2 is injected into coal seam, the reservoir pressure increases, enlarging the pressure generated between and production well. This drives CH_4 to diffuse and seepage toward production well. Because the sorption affinity of CO_2 is stronger than that of CH_4, the injected CO_2 will competitively adsorb with CH_4, replacing CH_4 on the adsorption site. Besides, the injected CO_2 with higher heat source will accelerate the transport rate of gas molecules, making the gas molecules move toward production well faster. After CO_2 transports to the production well, the pressure gradient between injection well and production well gradually decreases with time. The CH_4 content in coal seam changes relatively slow in

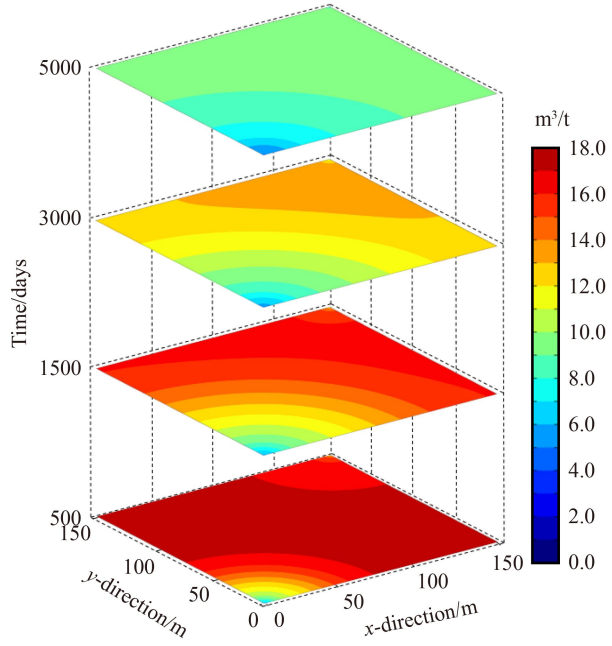

Fig. 6 CH_4 content in coal seam during CO_2-ECBM.

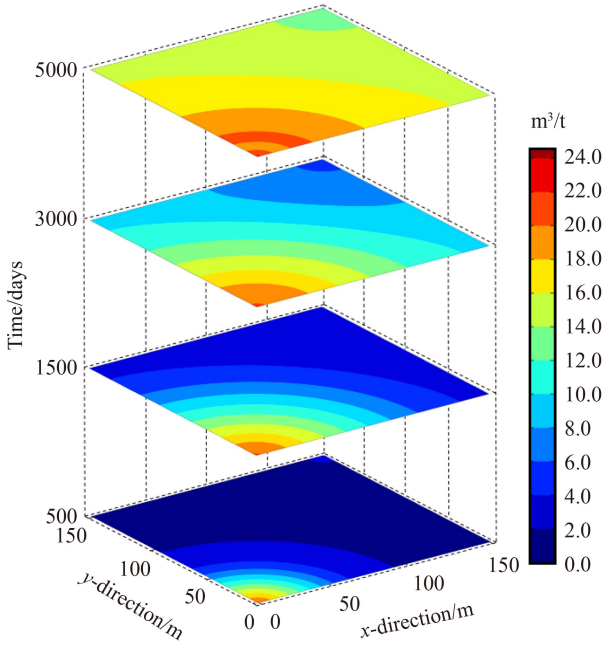

Fig. 8 Contour of CO_2 content during CO_2-ECBM.

the later stage as the most of CH_4 is extracted. Figure 7 presents the evolution of CH_4 content on the reference line AB during CO_2-ECBM recovery. Overall the CH_4 content shows a decreasing trend. In the early stage, the CH_4 content on the reference line AB reduces greatly. The slope of the curve of CH_4 content becomes small at later stage, indicating the small change of CH_4 content at this stage.

In Fig. 8, CO_2 continuously transports from the injection well toward the production well forced by the injection pressure. At 3000 day, the CO_2 content around the production well is significantly low, indicating that CO_2 has broken through the production well at this moment. In Fig. 9, the change of CO_2 content from injection well to production well shows a decreasing slight increasing decreasing trend. Overall, the CO_2 content increases gradually with time, e.g. it increases from 1.8 m^3/t to 16 m^3/t with an increasement of 8.9 times at point P.

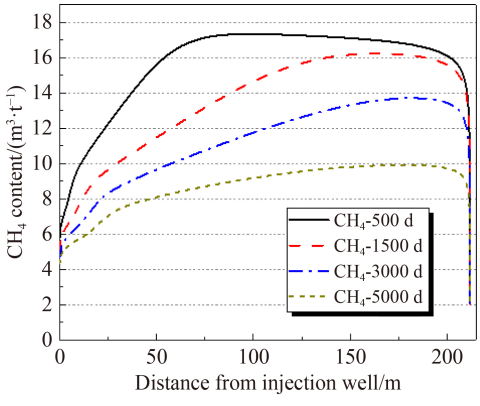

Fig. 7 CH_4 content on the reference line AB during CO_2-ECBM.

3.2.2 Permeability evolution

For regular drainage, the permeability on the reference line AB decreases in the early stage, but appears an overall upward trend with time, as shown in Fig. 10. The closer to the production well, the higher increase of the permeability. In the early stage, CH_4 pressure in coal seam gradually decreases leading to gradual increase of the effective stress which dominates the decrease of permeability. In the later stage, CH_4 concentration in the fractures becomes low, causing CH_4 desorption and matrix shrinkage, so as to increase the permeability in coal seam.

For CO_2-ECBM recovery, the permeability on the

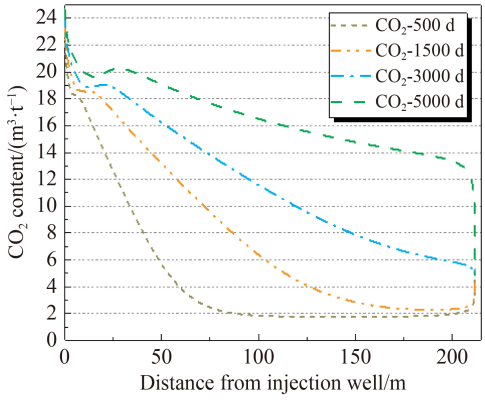

Fig. 9 Evolution of CO_2 content on the reference line AB during CO_2-ECBM.

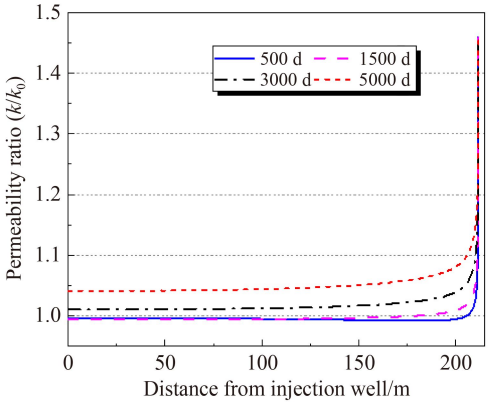

Fig. 10 Evolution of permeability on the reference line AB during regular drainage.

reference line AB shows a downward trend, with a faster variation near injection well, as shown in Fig. 11. This is because the arrival of CO_2 and heat flux brings adsorption swelling and thermal expansion of coal matrix, which occupies the fracture space and results in decrease of coal permeability. The range of permeability reduction gradually spreads over time.

3.2.3 CH_4 production and CO_2 sequestration

Figure 12 gives the gas rate of CH_4 production and CO_2 sequestration in a duration of 5000 d. The CH_4 production rate first increases rapidly and then decreases slowly. There are two peak points on the curve, with the first at the initial time caused by the rapid influx of free CH_4 from the fracture space in coal seam, and the second caused by the end of dewatering stage. For regular drainage, the highest production rate is 1555.3 m^3/t occurring at 680 d, while for CO_2-ECBM, the highest production rate is 1913.2 m^3/t occurring at 940 d. Due to the injection of CO_2, the peak CH_4 production is increased and delayed. The CH_4 production of CO_2-ECBM is always greater than that of regular drainage in

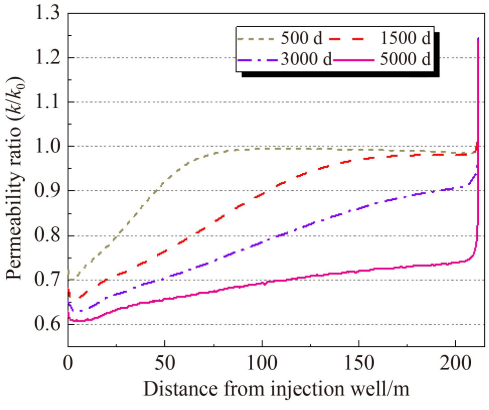

Fig. 11 Evolution of permeability on the reference line AB during CO_2-ECBM.

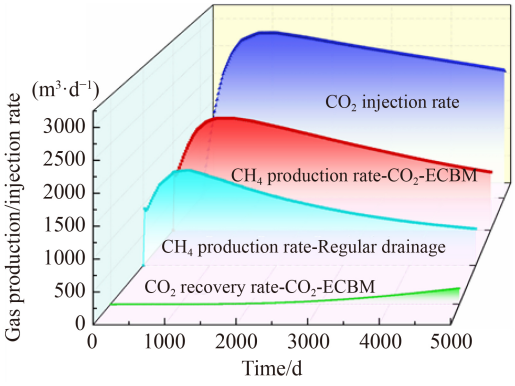

Fig. 12 Gas production/sequestration rate.

the whole process. The injection rate of CO_2 also shows a first increasing - then decreasing trend, with a peak point of 2940.3 m^3/t at 1200 d. The breakthrough of CO_2 occurs at 1460 d, and then the CO_2 rate starts to increase gradually.

In Fig. 13, the CH_4 cumulative production of both regular drainage and CO_2-ECBM increases linearly. At 5000 d, the CH_4 cumulative production of CO_2-ECBM is 7.1×10^6 m^3, comparing with 5.1×10^6 m^3 of regular drainage, with an increasement of 39.2%. This implies that CO_2 injection can effectively improve the CH_4 production from the coal reservoir. The cumulative CO_2 sequestration also increases linearly, reaching 11.7×10^7 m^3 at 5000 d. It can be concluded that the technology of CO_2 sequestration in the coal seam is feasible.

4 Optimization of start time for CO_2 injection

4.1 Injection/drainage scheme

In the CO_2-ECBM process, the premature start of CO_2 injection will lead to early CO_2 breakthrough in the production well, and reduce the calorific value in the

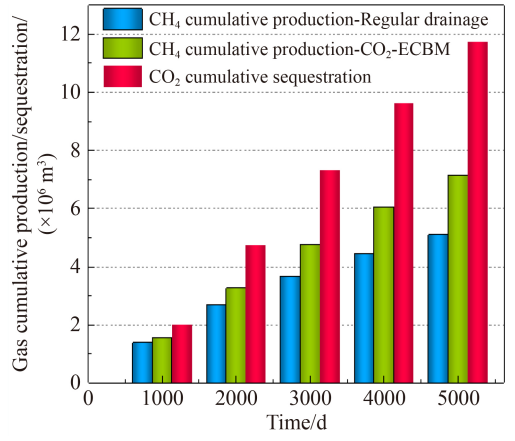

Fig. 13 Gas cumulative production/sequestration.

produce gas flow due to intrusive CO_2 mixture. And higher injection pressure is required to overcome the water resistance as the coal seam has not been dewatered. When the CO_2 injection is delayed, the fluid pressure in coal seam will be depleted, as a result the required injection pressure is reduced. In this case, high-calorie coalbed methane has already been recovered for a period of time until CO_2 breaks through. But, if the start time of CO_2 injection is too late, the CH_4 production cannot be improved, which is similar to regular drainage. Therefore, reasonable start time of CO_2 injection should be determined. In this section, the following scenarios are designed by changing the start time while keeping constant for other parameters. The injection well is also used for production during the CBM stage, and is modified to be an injection well at the appointed CO_2 injection start time. The injection/drainage scheme for optimizing of CO_2 injection start time is shown in Table 2.

4.2 Result analysis

The CH_4 and CO_2 production rates for different injection start times is shown in Fig. 14. The production rate of CH_4 first increases and then decreases during the CBM stage, and it decreases sharply when CO_2 injection starts to operate, which is caused by the change of gas production from two wells to a single well. After that, the production rate of CH_4 will enter a second small increase stage followed by a slow decrease. The first peak production rate is 3188.8 m^3/t occurring at 292 d. The CH_4 production rate shows a second peak after CO_2 injection, indicating that CO_2 injection can enhance the CH_4 production. When CO_2 injection starts, CO_2 migrates from the injection well to the production well. After a while of injection, the CO_2 breaks through at the production well, followed that the production rate of CO_2 gradually increases. The earlier the injection time of CO_2, the faster the production rate after the breakthrough. When the production rate of CO_2 reaches a certain value, the production well should be shut down considering the economic effect. To facilitate comparison with single-well production, in this paper, we define the threshold as the ratio of CO_2 recovery rate to CH_4 production rate of 15%. In the above 7 schemes, the time to shut down the production well are 4320, 4839, 5604, 6236, 6840, 7465, and 7676 d, respectively.

Table 2 Scheme for gas injection time optimization

Number	Specific measure
Case 1	IW injection CO_2, PW gas drainage
Case 2	Stage1 (CBM): IW + PW drainage 500 d, Stage 2 (ECBM): IW injection CO_2, PW drainage
Case 3	Stage1 (CBM): IW + PW drainage 1000 d, Stage 2 (ECBM): IW injection CO_2, PW drainage
Case 4	Stage1 (CBM): IW + PW drainage 1500 d, Stage 2 (ECBM): IW injection CO_2, PW drainage
Case 5	Stage1 (CBM): IW + PW drainage 2000 d, Stage 2 (ECBM): IW injection CO_2, PW drainage
Case 6	Stage1 (CBM): IW + PW drainage 2500 d, Stage 2 (ECBM): IW injection CO_2, PW drainage
Case 7	Stage1 (CBM): IW + PW drainage 3000 d, Stage 2 (ECBM): IW injection CO_2, PW drainage

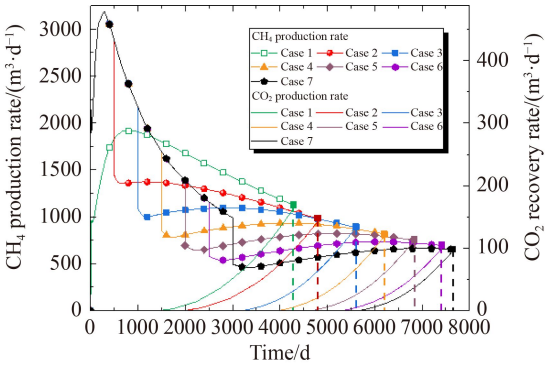

Fig. 14 Gas production rates at different injection start times.

Figure 15 shows the cumulative CH_4 production curves at different injection start times. When the production well is shut down, the cumulative CH_4 production for injection start time of 0, 500, 1000, 1500, 2000, 2500, and 3000 d are 6.42, 6.80, 7.45, 7.80, 8.10, 8.35, and 8.31 × 10^6 m^3, respectively. The cumulative CH_4 production also increases gradually with the prolong of injection start time, except for Case 7, which slightly decreases compared to Case 6.

Figure 16 shows the cumulative CO_2 sequestration for different injection start times. When the production well is shut down, the cumulative CO_2 sequestration is 10.35, 11.11, 11.38, 11.40, 11.39, 11.44, and 10.66 × 10^6 m^3, respectively. Figure 17 shows the variation law of CH_4 production/CO_2 sequestration and breakthrough time with the CO_2 injection start time. The breakthrough time increases gradually with the delay of injection time. The cumulative production of CH_4 continues to increase until slightly decreases at 2500 d. The cumulative CO_2 sequestration first increases slowly with the injection time, and remains stable from 1000 to 2500 d, and finally

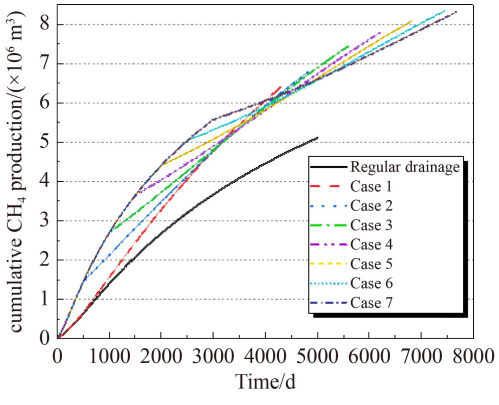

Fig. 15 Cumulative CH_4 production at different injection times.

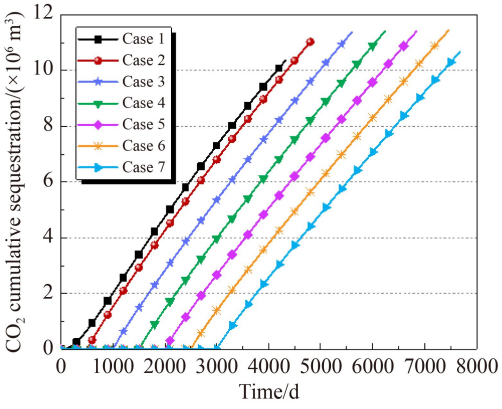

Fig. 16 CO_2 cumulative sequestration at different injection times.

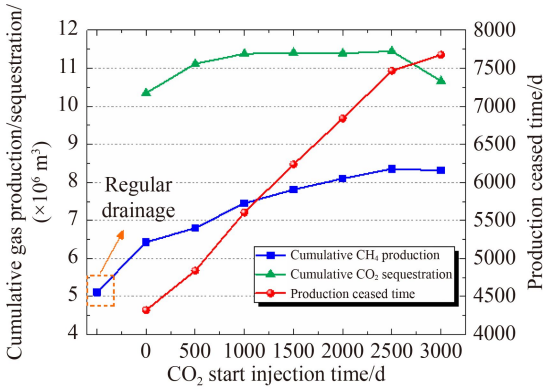

Fig. 17 Variation law of CH_4 production/CO_2 sequestration and breakthrough time with the CO_2 injection start time.

shows a decreasing trend after 2500 d. In summary, when the injection start time is 2500 d, the CH_4 cumulative/and CO_2 sequestration reaches the maximum before shut down. Hence, the optimal injection starting time in this research is 2500 d. Compared with the simultaneous start of drainage and injection, the scheme has improved the CH_4 drainage effect by an increment 30.1% of the cumulative CH_4 production.

5 Conclusions

The dual pore structure of coal mass, and the Weibull distribution of fracture permeability are assumed to propose an improved THM coupling mathematical model for CO_2-ECBM simulation. The model considers the non-isothermal adsorption of binary gases, dynamic gas diffusion between matrix and fractures, multiphase seepage, coal deformation, heat conduction and heat convection. The simulation on CO_2-ECBM recovery process is carried out by solving mathematical model via COMSOL Multiphysics software, and the following conclusions can be drawn.

1) The CH_4 content of CO_2-ECBM is significantly lower than that of regular drainage at the same time. The injected CO_2 competes adsorption with CH_4 by displacing the adsorption site, meanwhile drives CH_4 to diffuse and seepage more rapidly toward the production well. In addition, the CH_4 content in coal seam during CO_2-ECBM decreases rapidly in the early stage, but slowly in the later stage.

2) Coal seam permeability evolution is triggered by changes in gas adsorption/desorption, temperature and effective stress. For regular drainage, the early permeability shows a decreasing trend dominated by the increase of effective stress, while the later permeability shows an increasing trend dominated by the CH_4 desorption caused shrinkage of coal matrix. For CO_2-ECBM, the permeability in coal seam generally shows a downward trend due to superposition of matrix swelling induced by CO_2 adsorption and thermal expansion, particularly near injection well.

3) For both regular drainage and CO_2-ECBM, CH_4 production rate first rapidly increases and then slowly decreases. For CO_2-ECBM, an increased and delayed peak production rate of CH_4 appears, and the CH_4 production rate is always higher than that of regular drainage. The cumulative CH_4 production and CO_2 sequestration linearly increase with time, and the cumulative CH_4 production of CO_2-ECBM has increased by 39.2% in the duration 5000d compared with regular drainage.

4) A reasonable CO_2 injection start time can overcome early CO_2 breakthrough and ineffective increase of CH_4 production. In this study, the optimal injection start time is 2500 d, which has an increment of 30.1% for CH_4 cumulative production compared with the simultaneous injection.

References

Cheng L, Li D, Wang W, Liu J (2021). Heterogeneous transport of free CH_4 and free CO_2 in dual-porosity media controlled by anisotropic in situ stress during shale gas production by CO_2 flooding: implications for CO_2 geological storage and utilization. ACS Omega, 6(40): 26756–26765

Fan C J, Elsworth D, Li S, Chen Z W, Luo M K, Song Y, Zhang H H (2019b). Modelling and optimization of enhanced coalbed methane recovery using CO_2/N_2 mixtures. Fuel, 253: 1114–1129

Fan C J, Elsworth D, Li S, Zhou L J, Yang Z H, Song Y (2019a). Thermo-hydro-mechanical-chemical couplings controlling CH_4 production and CO_2 sequestration in enhanced coalbed methane recovery. Energy, 173: 1054–1077

Fan C J, Li S, Luo M K, Du W Z, Yang Z H (2017). Coal and gas outburst dynamic system. Int J Min Sci Technol, 27(1): 49–55

Fan C J, Wen H O, Li S, Bai G, Zhou L J (2022). Coal seam gas extraction by integrated drillings and punchings from the floor roadway considering hydraulic-mechanical coupling effect.

Geofluids, 2022: 5198227

Fan C J, Yang L, Wang G, Huang Q M, Fu X, Wen H O (2021a). Investigation on coal skeleton deformation law in CO_2 injection enhanced CH_4 drainage from underground coal seam. Front Earth Sci, 9: 891

Fan Y P, Deng C B, Zhang X, Li F Q, Wang X Y, Qiao L (2018). Numerical study of CO_2-enhanced coalbed methane recovery. Int J Greenh Gas Control, 76: 12–23

Fan Z L, Fan G W, Zhang D S, Zhang L, Zhang S, Liang S S, Yu W (2021b). Optimal injection timing and gas mixture proportion for enhancing coalbed methane recovery. Energy, 222: 119880

Fang H H, Sang S X, Liu S Q (2019a). Numerical simulation of enhancing coalbed methane recovery by injecting CO_2 with heat injection. Petrol Sci, 16(1): 32–43

Fang H H, Sang S X, Liu S Q (2019b). Establishment of dynamic permeability model of coal reservoir and its numerical simulation during the CO_2-ECBM process. J Petrol Sci Eng, 179: 885–898

Fang H H, Sang S X, Liu S Q (2019c). The coupling mechanism of the thermal-hydraulic-mechanical fields in CH_4-bearing coal and its application in the CO_2-enhanced coalbed methane recovery. J Petrol Sci Eng, 181: 106177

Hou Y D, Huang S P, Han J, Liu X B, Han L F,Fu C F (2020). Numerical simulation of the effect of injected CO_2 temperature and pressure on CO_2-enhanced coalbed methane. Appl Sci (Basel), 10(4): 1385

Huo B J, Jing X D, Fan C J, Han Y L (2019). Numerical investigation of flue gas injection enhanced underground coal seam gas drainage. Energy Sci Eng, 7(6): 3204–3219

Liu A, Liu S M, Liu P, Wang K (2021a). Water sorption on coal: effects of oxygen-containing function groups and pore structure. Int J Coal Sci Technol, 8(5): 983–1002

Liu J S, Chen Z W, Elsworth D, Miao X X, Mao X B (2011). Evolution of coal permeability from stress-controlled to displacement-controlled swelling conditions. Fuel, 90(10): 2987–2997

Liu J, Xie L, Elsworth D, Gan Q (2019). CO_2/CH_4 competitive adsorption in shale: implications for enhancement in gas production and reduction in carbon emissions. Environ Sci Technol, 53(15): 9328–9336

Liu J, Yao Y B, Liu D M, Elsworth D (2017). Experimental evaluation of CO_2 enhanced recovery of adsorbed-gas from shale. Int J Coal Geol, 179: 211–218

Liu M Y, Wen H, Fan S X, Wang Z P, Fei J B, Wei G M, Cheng X J, Wang H (2022). Experimental Study of CO_2-ECBM by injection Liquid CO_2. Minerals (Basel), 12(3): 297

Liu T, Lin B Q, Fu X H, Liu A (2021b). Mechanical criterion for coal and gas outburst: a perspective from multiphysics coupling. Int J Coal Sci Technol, 8(6): 1423–1435

Luo M K, Yang L, Wen H O, Zhao D S, Wang K (2022). Numerical optimization of drilling parameters for gas predrainage and excavating-drainage collaboration on roadway head. Geofluids, 2022: 3241211

Mu Y L, Fan Y P, Wang J R, Fan N (2019). Numerical study on the injection of heated CO_2 to enhance CH_4 recovery in water-bearing coal reservoirs. Energy Sources A Recovery Util Environ Effects

Niu Q H, Wang W, Liang J J, Yuan W, Wen L, Chang J F, Ji Z M, Zhou H, Wang Z Z, Jia X J (2020). Investigation of the CO_2 flooding be havior and its collaborative controlling factors. Energy Fuels, 34(9): 11194–11209

Ren T, Wang G, Cheng Y P, Qi Q X (2017). Model development and simulation study of the feasibility of enhancing gas drainage efficiency through nitrogen injection. Fuel, 194: 406–422

Sun Y F, Zhao Y X, Yuan L (2018). CO_2-ECBM in coal nanostructure: modelling and simulation. J Nat Gas Sci Eng, 54: 202–215

Vishal V, Singh T N, Ranjith P G (2015). Influence of sorption time in CO_2-ECBM process in Indian coals using coupled numerical simulation. Fuel, 139: 51–58

Wang G, Wang K, Wang S G, Elsworth D, Jiang Y J (2018). An improved permeability evolution model and its application in fractured sorbing media. J Nat Gas Sci Eng, 56: 222–232

Wang Z L, Sang S X, Zhou X Z, Liu X D (2022). Numerical study on CO_2 sequestration in low-permeability coal reservoirs to enhance CH_4 recovery: gas driving water and staged inhibition on CH_4 output. J Petrol Sci Eng, 214: 110478

Wu Y, Liu J S, Chen Z W, Elsworth D, Pone D (2011). A dual poroelastic model for CO_2-enhanced coalbed methane recovery. Int J Coal Geol, 86(2–3): 177–189

Xia T, Zhou F, Gao F, Kang J, Liu J, Wang J (2015). Simulation of coal self-heating processes in underground methane-rich coal seams. Int J Coal Geol, 141-142: 1–12

Xiao B, Liu S G, Li Z W, Ran B, Ye Y H, Yang D, Li J X (2021). Geochemical characteristics of marine shale in the Wufeng Formation–Longmaxi Formation in the northern Sichuan Basin, South China and its implications for depositional controls on organic matter. J Petrol Sci Eng, 203: 108618

Zhang L, Li J H, Xue J H, Zhang C, Fang X Q (2021). Experimental studies on the changing characteristics of the gas flow capacity on bituminous coal in CO_2-ECBM and N_2-ECBM. Fuel, 291: 120115

Zhang X G, Ranjith, P G (2019). Experimental investigation of effects of CO_2 injection on enhanced methane recovery in coal seam reservoirs. J CO_2 Util, 33: 394–404

Zhao P, He B, Zhang B, Liu J (2022). Porosity of gas shale: is the NMR-based measurement reliable? Petrol Sci, 19(2): 509–517

Zheng S J, Yao Y B, Elsworth D, Liu D M, Cai Y D (2020). Dynamic fluid interactions during CO_2-ECBM and CO_2 sequestration in coal seams. Part 2: CO_2-H_2O wettability. Fuel, 279: 118560

Zheng S J, Yao Y B, Sang S X, Liu D M, Wang M, Liu S Q (2022). Dynamic characterization of multiphase methane during CO_2-ECBM: an NMR relaxation method. Fuel, 324: 124526

Zhou F D, Hussain F, Cinar Y (2013). Injecting pure N_2 and CO_2 to coal for enhanced coalbed methane: experimental observations and numerical simulation. Int J Coal Geol, 116-117: 53–62

Zhou L J, Zhou X H, Fan C J, Bai G (2022). Coal permeability evolution triggered by variable injection parameters during gas mixture enhanced methane recovery. Energy, 252: 124065

Zhu Z J, Yao Z H, Nemcik J, Han J (2022). Investigation of overburden movement and ground stress behaviour in multiseam mining. Lithosphere, 2022(special 11): 3312379